PREPARATION OF PEROVSKITE-TYPE $ZnSnO_3$ NANOPARTICLES AND ENHANCING THEIR BEHAVIOR AS A POSITIVE ELECTRODE FOR SUPERCAPACITOR APPLICATIONS.

***Morad, M. M.*[*]; Mohamed, S. G.[†,§]; AbouShahba, R. M.*[*] and Rashad, M. M.*[‡]**

[*] *Chemistry Department, Faculty of Science (Girls), Al-Azhar University, Cairo 11751, Egypt.*

[†] *Mining and Metallurgy Engineering Department, Tabbin Institute for Metallurgical Studies, (TIMS), Tabbin, Helwan 109, Cairo 11421, Egypt.*

[‡] *Electronic and Magnetic Materials Department, Advanced Materials Institute, Central Metallurgical Research and Development Institute (CMRDI), P.O. Box 87 Helwan, Cairo, Egypt.*

[§] *Corresponding Author; E-mail: sgmmohamed@gmail.com (S. G. Mohamed).*

ABSTRACT

This work aims to prepare perovskite zinc stannate ($ZnSnO_3$) by the sol-gel method and to study the electrochemical properties. This performance improves by adding different percentages of naturally prepared activated carbon from pomegranate peels. $ZnSnO_3$ is considered an attractive cathode material for energy storage, which shows a specific capacitance of 115 F g^{-1} at 1 A g^{-1}, while the optimum added percentage of the activated carbon is 5%AC+95%$ZnSnO_3$, which exhibits 312.5 F g^{-1} at the same current density, which considered about three times more than that of the $ZnSnO_3$, with capacitance retention of 66% after 2000 cycles at the current density of 10 A g^{-1}. The practical hybrid device shows a specific capacitance value of 61.6 F g^{-1} at 1 A g^{-1}, the specific energy of 22 Wh $kg^{-1,}$ and specific power of 1077 W kg^{-1} with capacitance retention of 50% of the initial capacitance after 2000 cycles at a current density of 10 A g^{-1}. As a result, $ZnSnO_3$ and its composite with cheap and natural materials are considered promising supercapacitor electrodes.

Keywords

Perovskite $ZnSnO_3$; Activated carbon; Sol-gel method; hybrid device; supercapacitor electrode.

1. INTRODUCTION

Great efforts of green energy devices and researchers have been made to overcome the ever-growing energy crisis and environmental pollution by converting environmental waste into useful material for energy storage systems such as supercapacitors [1-6]. Electrochemical energy storage devices are classified into electrochemical double-layer capacitors (EDLCs), Pseudocapacitors, and hybrid capacitors [7-9]. Currently, most of the research focuses on supercapacitors to obtain advanced electrode materials with higher specific capacitance and more extended cycling stability, as an essential ternary semiconducting oxide, mostly ABO_3 type ($ZnSnO_3$), has been attracting most of the studies due to its different applications in various fields, such as gas sensor [10, 11], photo-catalyst [12], and lithium-ion batteries [13]. A few studies have reported $ZnSnO_3$ as a supercapacitor due to their low thermal stability than Zn_2SnO_4; with a focus on charge storage applications, it is undeniable that stannate has proved very effective in sensor and charge storage technologies [14-22]. The main reasons are phase

stabilization in $ZnSnO_3$ and structural complexities in Zn_2SnO_4 [23, 24]. In the ZnO: SnO_2 system at normal pressure, two phases exist; stable Zn_2SnO_4 and metastable $ZnSnO_3$ [25, 26]. Zn_2SnO_4 has a spinal structure and can be easily synthesized by a simple solid-state reaction method or another method. It has high thermal stability and has been chemically and structurally characterized [27]. Comparatively, reports on $ZnSnO_3$ are sparse and ambiguous, owing to its low thermal stability and challenging synthesis methods [15].

Lower thermal stability of $ZnSnO_3$ also results in its decomposition into Zn_2SnO_4, ZnO, and SnO_2 at higher temperatures. Therefore, low-temperature synthesis techniques like co-precipitation and hydrothermal synthesis were employed to overcome the problems mentioned above. However, these techniques have low sample output to input ratio and are less industry-friendly. Consequently, the sol–gel method can overcome this problem, giving the appropriate amount of the $ZnSnO_3$ required. During the past decades, perovskite oxides (ABO_3), such as $SrRuO_3$ [28], $BiFeO_3$ [29], etc., have been reported as potential electrode materials for supercapacitors. However, most of the reported perovskite oxides exhibit unsatisfactory electrochemical properties, limiting their further applications. Therefore, exploring new-type of perovskite candidates becomes highly valuable for high-performance supercapacitors like $ZnSnO_3$ as well as carbon-based materials [30], metal oxides [31], metal sulfides [32], and conducting polymers [33] are used as supercapacitor electrode materials [34-36]. Carbon materials have been used from the beginning of supercapacitor fabrication due to their high surface area. Metal oxides offer attractive options as electrode material due to high specific capacitance and low resistance, making it easier to construct high-energy and power supercapacitors. Few studies reported the usage of zinc stannate for supercapacitors application; Sim *et al.* [37, 38] reported the synthesis and supercapacitive behavior of $ZnSnO_3$@carbon composite and $ZnSnO_3$/mesoporous carbon composite, which showed only specific capacitance of 104 and 94 F g^{-1}, respectively, at a low current density of 0.3 A g^{-1}.

This work investigated perovskite zinc stannate's electrochemical performance and improved performance by mixing it with different percentages of naturally prepared activated carbon from waste material with a higher surface area. The morphological and surface area properties were studied as they play a critical role in the ions' adsorption and diffusion during the electrochemical process. Detailed electrochemical studies were conducted on a single electrode and a practical symmetrical device. $ZnSnO_3$ was obtained with a surface area of 4.064 m^2 g^{-1} with a microporous characteristic. 5%AC+95%ZnSnO3 exhibited an excellent electrochemical feature with a remarkable specific capacitance of 312.5 F g^{-1} at 1 A g^{-1} with good cycling stability of 66% capacitance retention after 2000 cycles at a current density of 10 A g^{-1}, which improved energy storage life.

2. EXPERIMENTAL METHODS

2.1. Preparation of $ZnSnO_3$ Nanoparticles

Polycrystalline perovskite-type $ZnSnO_3$ nanoparticles were synthesized by sol-gel method at atmospheric pressure using stoichiometric amounts of high purity Zinc Acetate ($Zn(CH_2COOH)_2$), Tin (IV) Chloride ($SnCl_4.5H_2O$), and fuel (EDTA). The

starting materials were dissolved in 50 ml of distilled water to form transparent homogenous precursors. The precursors were magnetically stirred for 3 h (condensation time) at 300°C and were immediately mixed to form a milky white solution. Mixing was followed by adding 5 ml of Ethylene Glycol and a few drops of NH_3 until pH control of the solution (pH~7). The grayish-brown powder obtained after drying the solution in the air was ground, and the obtained powder was calcined for 3 h at 400ºC.

2.2. Materials Characterization

The as-prepared materials were characterized by powder X-ray diffraction (XRD, Brucker D8 diffractometer) using the Cu-Kα (λ=1.5406A0) radiation and secondary monochromator in the range 2θ from 10 to 70° and a scan rate of 20 min^{-1}. The morphologies were characterized by a field emission scanning electron microscope (FSEM) using a JEOL instrument (JSM –5410, Japan). The chemical compositions and the valence states of the elements were determined by X-ray photoelectron spectroscopy (XPS, thermos scientific) using Al Kα monochromatized radiation. The specific surface areas were calculated by the Brunauer–Emmett–Teller (BET) method. Quanta chrome NovaWin - Data Acquisition and Reduction for NOVA instruments ©1994-2013, Quanta chrome Instruments version 11.03.

2.3. Electrochemical Measurements

To evaluate the electrochemical properties of the prepared samples using a 3-electrode configuration in 6 M KOH solution as electrolyte. The working electrode was fabricated by adding the prepared active material with carbon black (conductive additive) and Nafion as a binder in a weight ratio of 80:10:10, respectively. Then 0.5 ml of ethanol was added to the mixture to produce a suspended solution. The working electrode was fabricated by the drop-casting method, and the suspended solution was dropped into nickel foam substrate (NF) with the dimensions of 1 cm (width), 2 cm (length), and 1.6 mm (thickness). The prepared film was then dried at 70°C overnight. The electrochemical behavior of the prepared material was tested by a three-electrode system using an electrochemical testing station (Volta lab 40 PGZ 301, Radiometer Analytical, France) at room temperature, with a platinum wire as a counter electrode and saturated calomel electrode (SCE) as a reference electrode. The electrochemical measurements were performed in a 6 M KOH aqueous solution electrolyte. For practical application, an asymmetric hybrid device (ASHD) was assembled, in which the perovskite zinc stannate was used as a positive electrode and the activated carbon (AC) as a negative electrode. According to the previous report, [39]. The ASHD was denoted as (95% $ZnSnO_3$ + 5% AC)//AC). The electrochemical measurements were performed using cyclic voltammetry (CV), galvanostatic charge-discharge (GCD), and electrochemical impedance spectroscopy (EIS) measurements. The CV measurements were carried out within a potential window of -0.1 to 0.6V (vs. SCE) at different scan rates from 10 to 200 mV s^{-1}. GCD measurements were tested at different current densities from 1 to 10 A g^{-1} within a potential window of 0 to 0.4 V (vs. SCE). The EIS measurements were performed using Nyquist plots in the frequency range of 100 kHz to 0.01 Hz. The stability test was carried out at a current density of 10 A g^{-1}. The specific capacitance (Csp) F g^{-1} was then calculated from the GCD results according to the following equation: [40, 41]

$$C_{sp} = 2\,I \int V\,dt / m\,\Delta V^2 \quad (1)$$

Where I is the applied current (A), Δt is the discharging time (s), ΔV is the potential window (V), and m is the mass of active material (g). For fabrication of battery-like ASHD, the (95% $ZnSnO_3$ - 5% AC) was used as a positive electrode and AC as a negative electrode. The following equation can calculate the mass ratio of positive and negative electrodes (m^+/ m^-) [42].

$$m^+/m^- = C_{sp} - \Delta V^-/C_{sp} + \Delta V^+ \quad (2)$$

Where C_{sp} (-) and C_{sp} (+) are the capacitances of the negative and positive electrode, respectively, and ΔV^- and ΔV^+ are the potential windows of the negative and positive electrode, respectively. The CV measurements of the device were carried out within a voltage window of 0 to 1.6 V at different scan rates from 10 to 200 mV s^{-1}. GCD measurements were tested at different current densities from 1 to 10 Ag^{-1} between voltage windows of 0 to 1.6 V. The energy density (Ed) and power density (Pd) of the device were calculated according to the equations, respectively. [43, 44]

$$Ed = I \int V\, dt/3.6m \quad (3)$$

$$Pd = 3600\, Ed/td \quad (4)$$

Where Ed is the energy density (Wh kg^{-1}), dt is discharge time (s), Pd is the power density (W kg^{-1}), and (V) is the operating voltage window of the device.

3. RESULTS AND DISCUSSION

3.1. Structural and Morphological of the Synthesized $ZnSnO_3$ Nanoparticles

The X-ray diffraction patterns of samples shown in Figure 1a indicate that sample calcined at 400°C for 3 h with EDTA as fuel yields a pure phase with no detectable secondary phase. All the peaks were ascribed to ilmenite type $ZnSnO_3$ (JCPDS card no. 28-1486). The crystal structure of $ZnSnO_3$ can be regarded as a cubic phase. Crystallite size was automatically calculated from X-ray diffraction data using Debye- Scherrer equation; Wf = 0.9 λ\ D cos θD Where Wf is the width at half –maximum intensity of Bragg reflection excluding instrumental broadening, λ the wavelength of the X-ray radiation, D the average crystallite size, θD the Bragg angle. Considering the major peaks in the XRD pattern, the average crystallite size was calculated as 95.6 nm. Figure1b shows XPS spectra of O1s, with a mean peak with a small shoulder at a high binding energy side. The OI is attributed to lattice oxygen O_2 is ascribed to surface O_2, O, OH groups, and oxygen vacancies [45]. As shown in Figure 1c, we can clearly find the peaks at 1021.5 eV and 1044.5eV, consistent with the binding energy of Zn 2p3/2 and Zn 2p1/2. The splitting energy of 23 eV between Zn 2p3/2 and Zn 2p1/2 is a typical value for Zn in the $ZnSnO_3$. Meanwhile, the high-resolution XPS spectra of Sn 3d5/2 and Sn3d3/2 in Figure 1d are obviously observed at 486.9 eV and 495.5eV, respectively, which correspond to the Sn^{4+} [46]. Figures 2a and b reveal the nitrogen adsorption isotherm of the prepared oxide. The BET surface area was calculated from the nitrogen adsorption isotherm in the P/P0 range from 0.01 to 0.1 at room temperature; the obtained BET surface area is 4.064 $m^2\ g^{-1}$. The BET curve exhibits the typical type I isotherms according to the IUPAC classification [48], indicating the microporous feature of this sample, the average pore diameter is 2.8 nm. Figures 3a and

b show the FESEM image of the $ZnSnO_3$ nanoparticles, which revealed the formation of cubic shaped and some irregular shaped nanoparticles, From the FESEM image, it is visible that prepared $ZnSnO_3$ nanoparticles were pure with no impurities.

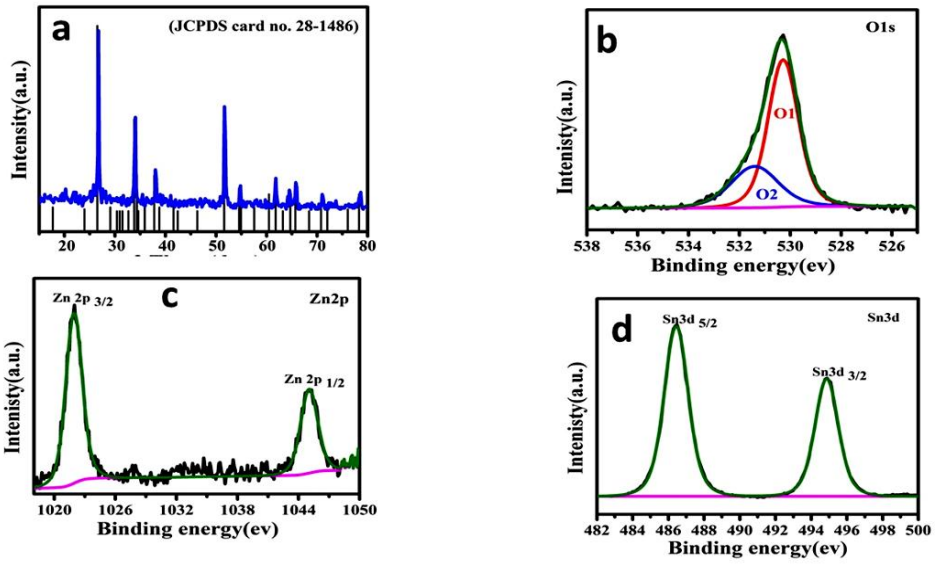

Fig. 1: (a) XRD pattern, and (b, c, d) High-resolution XPS spectra of $ZnSnO_3$.

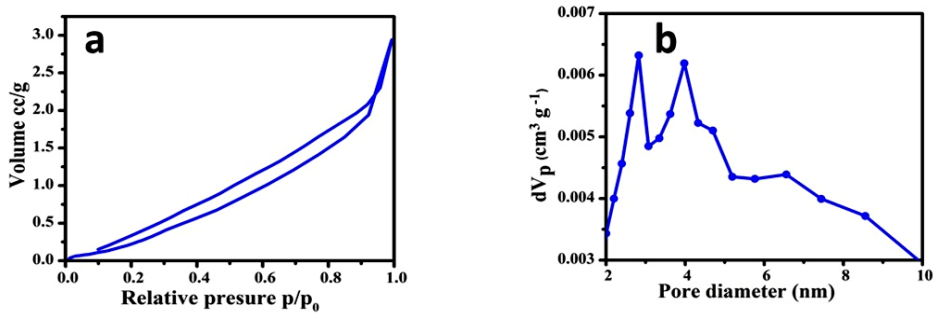

Fig. 2: (a) N_2 adsorption-desorption isotherms and (b) pore size distributions of $ZnSnO_3$.

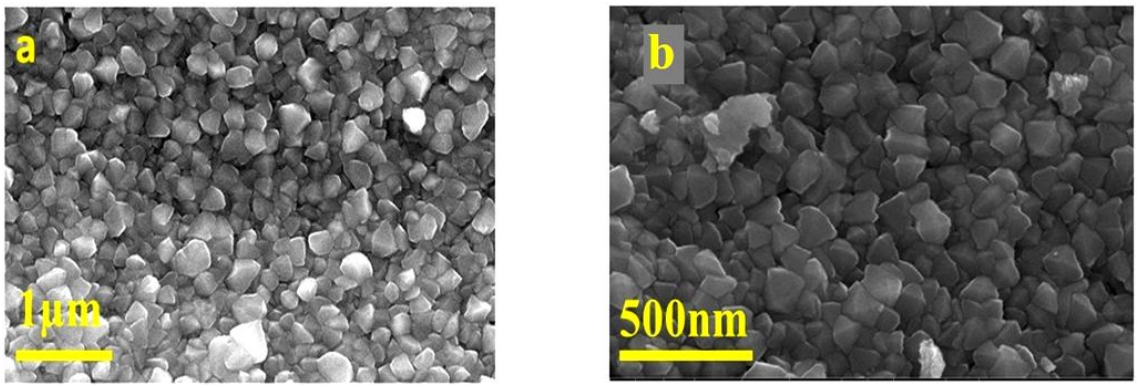

Fig. 3: (a, b) FE-SEM images of the as-prepared Zn_2SnO_4 with different magnifications.

3.2. Electrochemical Performance of the Supercapacitor Electrodes

To examine the electrochemical properties CV, GCD, and EIS were measured in 6 M KOH, of the as-prepared $ZnSnO_3$ and different ratios (3,5,10) % of natural prepared activated carbon mixed with prepared $ZnSnO_3$ to form other composites as an active electrode materials for SCs, It can be seen from figure 4a that, CV profiles of different ratios of $ZnSnO_3$ + AC composite and blank $ZnSnO_3$ operated at 50 mV s^{-1} and potential range of -0.1 to 0.6V which illustrate the oxidation and reduction peaks as a result of the faradic reactions between Sn(II)- Sn(III) -Sn(IV), as a result of CV profiles 5% AC + 95% $ZnSnO_3$ composite was considered to be the best ratio with high capacitance more than the blank $ZnSnO_3$, In order to evaluate the effect of scan rate on the electrochemical performance, the CV profiles of 5% AC + 95% $ZnSnO_3$ composite were performed at different scan rates, as illustrated in figure 4b, At low scan rates, the redox peaks are symmetrical, indicating the excellent reversibility of redox reaction at the surface of 5% AC + 95% $ZnSnO_3$ composite. With the increasing scan rate, it is observed that the shifting of anodic peaks towards the more positive position and the corresponding cathodic peaks towards a more negative position due to the electrode polarization as well as the sluggish diffusion rate of the electrolyte at high scan rates that is required to fulfill the electrochemical reactions of the electrode material [41]. However, the redox reaction peaks of the CV curves maintained their well-defined and sharp behavior, implying that these materials are suitable for fast redox reactions and possess better reversibility, which is significantly essential for power systems [47]. For an in-depth evaluation of the actual value of capacitance, we tested the charge-discharge profiles of the prepared 5% AC + 95% $ZnSnO_3$ hybrid composite at different current densities ranges from 1- 10 A g^{-1} in the potential range of 0 to 0.4V. As shown in Figure 3c, it is clear that the GCD curves exhibit apparent voltage plateaus, indicating that the supercapacitive performance is a Faradic-type. The presence of plateaus in the curves further confirms the existence of redox reaction, which is consistent with the results obtained from the CV curves. Csp was calculated from GCD measurements. Figure 4c also illustrates the effect of different current densities on performance; it is clear that all GCD curves exhibit apparent voltage plateaus, further demonstrating the Faradic-type supercapacitive performance. As a result of the comparison between values of the calculated capacitance of 5% AC + 95% $ZnSnO_3$ hybrid composite and $ZnSnO_3$ electrodes, as shown in figure 4d, which are 312.5 and 115 F g^{-1} at the current density of 1 A g^{-1}, respectively, presenting the capacitance of the 5% AC + 95% $ZnSnO_3$ hybrid composite electrode is about three times more than that of the $ZnSnO_3$. This result indicates a superior enhancement of the electrochemical performance of perovskite $ZnSnO_3$ as supercapacitor electrode by adding to the activated carbon from a natural source. For measuring cycle life stability of 5%AC+95%$ZnSnO_3$ hybrid composite and $ZnSnO_3$ electrodes, GCD measurements were operated at 10 A g^{-1} for 2000 cycles. The percentage of capacitance retention of 5% AC + 95% $ZnSnO_3$ hybrid composite and $ZnSnO_3$ electrodes were 66 and 53%, respectively, as shown in figure 4e. EIS was obtained at the open-circuit voltage, and the corresponding Nyquist plots are displayed in figure 4f. At the high-frequency region, the intersection of the curve at the real part (Zr) represents the equivalent series resistance (ESR), which is related to ionic resistance of the electrolyte, internal resistance of the electrode active material, and the contact resistance between the electrode and the current collector [48]. From the plots, the blank $ZnSnO_3$ electrode shows more value of ESR (2.43 ohm) than the 5% AC +

95% $ZnSnO_3$ hybrid composite (1.48 ohm) after the stability test, indicating the absence of the ohmic loss upon cycling due to high conductivity of activated carbon and opening more active site on the surface of composite electrode which improves EIS. The Nyquist plots show a semicircle in the high-frequency region and a near-vertical line at low frequency. The near-vertical line in the low-frequency region indicates the good capacitive of the composite electrode.

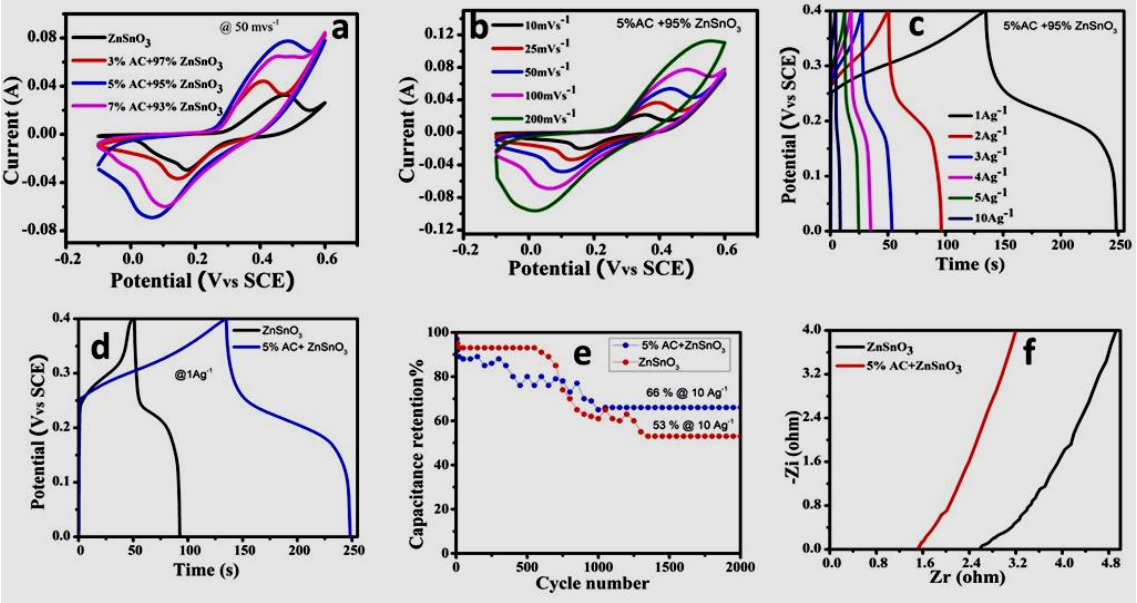

Fig. 4: (a) CV curves at scan rate from 50 mV s^{-1} (b) CV Curves of 5% composite at different scan rate from 10 to 200 mV s^{-1} (C) GCD curves at different current density from 1 to 10 Ag^{-1} for 5 % composite (d) GCD curves of blank $ZnSnO_3$ and 5% Composite at 1 Ag^{-1} .(e) Cycling stability of at a current density of 10 A g^{-1} of blank $ZnSnO_3$ and 5% Composite , and (f) EIS profile of blank $ZnSnO_3$ and 5% Composite electrodes.

3.3. Asymmetric Supercapacitor Device

For real simulation, a battery type of asymmetric device was fabricated in 6 M KOH electrolyte using two electrodes, 5% AC + 95% $ZnSnO_3$ hybrid composite as anode and naturally prepared AC as the cathode to evaluate the energy storage capacity of this hybrid composite in the complete supercapacitor cell. According to the mass balance equation, the mass ratio of the positive and negative electrode materials is 2, Eq. 2 (Csp(-) was calculated from the GCD profile Figure 4d). The operation potential of the prepared device can be calculated as the sum of the potential windows of 5% AC + 95% $ZnSnO_3$ (-0.1 to 0.6 V) and AC (-1 to 0 V). Therefore, a potential operation window of 0 to 1.6 V. The CV curves recorded at different scan rates from 10 mV s^{-1} to 200 mV s^{-1} for asymmetric supercapacitor in the potential range of 0 to 1.6 V is shown in figure 5a. As shown in Figure 5a, in all CV curves of the asymmetrical supercapacitor, the redox peaks were still noticeable in all CV curves, indicating the Faradic-type (battery-like) behavior of the 5% AC + 95% $ZnSnO_3$ composite//AC hybrid device. For more evidence, GCD measurements of the device, figure 5b, were performed at different current densities of 1, 2, 3, 4, 5, 10 A g^{-1}, which show a nonlinear battery type charge-discharge profile. The hybrid device offers a specific capacitance value of 61.6 F g^{-1} at 1

A g^{-1}, Ed of 22 Wh $kg^{-1,}$ and Pd of 1077 W kg^{-1}. The capacitance retention of the as-fabricated hybrid asymmetric device was operated at a current density of 4 Ag^{-1} within 0 to 1.6 V by the GCD test. As shown in Figure 5c, the hybrid device of 5% AC + 95% $ZnSnO_3$ composite//AC exhibits stability of 50% capacitance retention of the initial capacitance after 2000 cycles. EIS was also tested as in Figure 5d, which showed an ESR value of 2.5 ohm for fresh device electrode and 1.73 Ohm after the stability test, revealing that, after stability, EIS improved due to the absence of the ohmic loss upon cycling due to high conductivity of activated carbon and opening more active site on the surface of the composite electrode. Finally, electrochemical results indicate that the 5% AC + 95% $ZnSnO_3$ composite//AC hybrid device works as a battery-type capacitor and has excellent potential as an energy storage material.

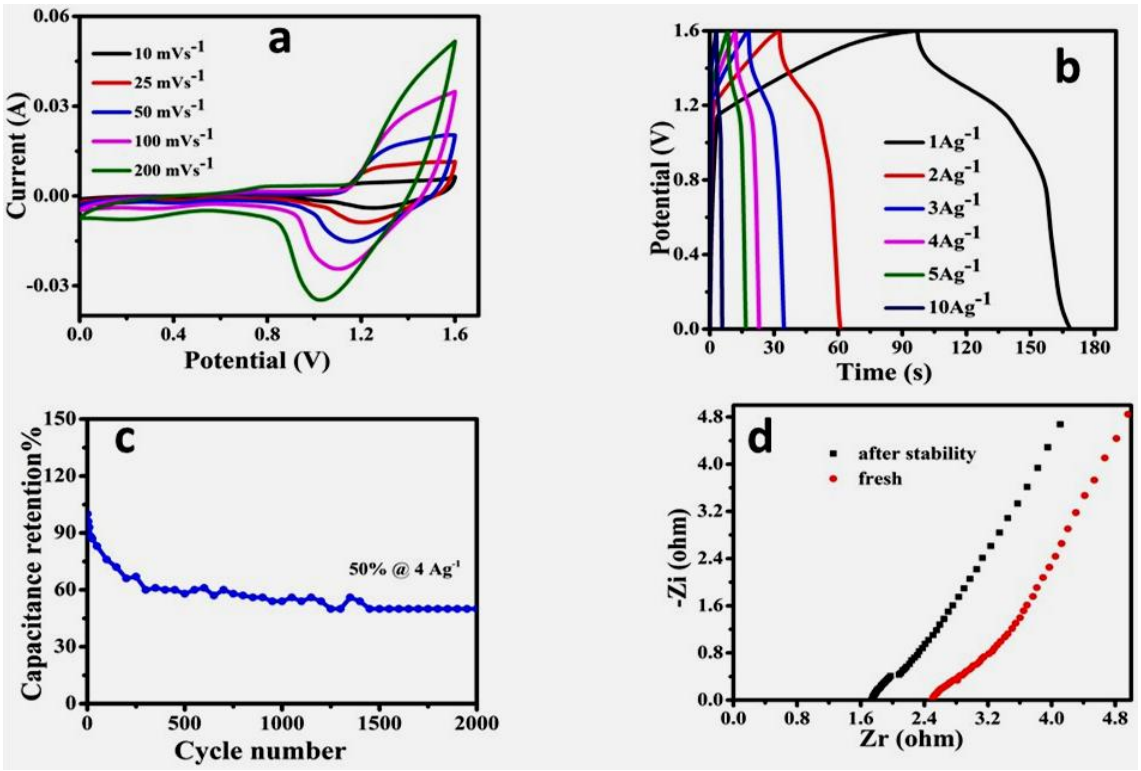

Fig. 5: Electrochemical performance of the 5% AC + 95% $ZnSnO_3$ composite //AC hybrid device (a) CV curves at different scan rates, (b) GCD curves at different current densities, (c) cycling performance at a current density of 4 A $g^{-1,}$ and (d) EIS for the fresh device and after 2K cycles.

4. CONCLUSIONS

In summary, a sol-gel method was used as a facile method to prepare $ZnSnO_{3,}$ which overcame the lack of quantity and produced low time and temperature are used, giving the appropriate amount of the $ZnSnO_3$ required. Due to the excellent conductivity of activated carbon and high capacitive $ZnSnO_3$, a different percentage of $ZnSnO_3$/AC composites are successfully obtained by well mixing. The value of specific capacitance obtained for $ZnSnO_3$ and 5% AC + 95% $ZnSnO_3$ hybrid composite is 115 and 312.5 F g^{-1} at 1 A g^{-1}, respectively, improving the electrochemical behavior of perovskite $ZnSnO_3$

with capacitance retention of 66% after 2000 cycles at a current density of 10 Ag^{-1}. Meanwhile, the practical simulation of the asymmetrical hybrid device shows a specific capacitance value of 61.6 F g^{-1} at 1 A g^{-1}, Ed of 22 Wh $kg^{-1,}$ and Pd of 1077 W kg^{-1}.with capacitance retention of 50% of the initial capacitance after 2000 cycles at a current density of 10 A g^{-1}, from this result we reached to the main goal by improving electrochemical properties by mixing with cheap and natural materials which used anode material for supercapacitor applications.

Declaration of interests

All authors declare that they have no conflicts of interest.

5. REFERENCES

[1] Winter, M. and Brodd, R. J.: Chem. Rev., "What Are Batteries, Fuel Cells, and Supercapacitors?". (Chem. Rev. 2003, 104, 4245−4269. Published on the Web 09/28/2004.) 1021-1021, 105 (2005).

[2] Liu, C.; Li, F.; Ma, L. P. and Cheng, H. M.: Adv. Mater., "Advanced materials for energy storage". E28-E62, 22 (2010).

[3] Zhang, Y.; Li, L.; Su, H.; Huang, W. and Dong, X.: J. Mater. Chem. A, "Binary metal oxide: advanced energy storage materials in supercapacitors". 43-59, 3 (2015).

[4] Tyagi, A.; Tripathi, K. M. and Gupta, R. K.: J. Mater. Chem. A, "Recent progress in micro-scale energy storage devices and future aspects". 22507-22541, 3 (2015).

[5] Thakur, V. K. and Gupta, R. K.: Chem. Rev., "Recent progress on ferroelectric polymer-based nanocomposites for high energy density capacitors: synthesis, dielectric properties, and future aspects". 4260-4317, 116 (2016).

[6] Ali, G. A.; Habeeb, O. A.; Algarni, H. and Chong, K. F.: J. Mater. Sci., "CaO impregnated highly porous honeycomb activated carbon from agriculture waste: symmetrical supercapacitor study". 683-692, 54 (2019).

[7] Najib, S. and Erdem, E.: Nanoscale Adv., "Current progress achieved in novel materials for supercapacitor electrodes: mini review". 2817-2827, 1 (2019).

[8] Elsaid, M. A. M.; Sayed, A. Z.; Ashmawy, A. M.; Hassan, A. A.; Waheed, A. F. and Mohamed, S. G.: The Bulletin Tabbin Institute for Metallurgical Studies (TIMS), "Hierarchically Nanocoral Reefs-like $ZnCo_2S_4$ Deposited on Ni Foam as an Electrode Material for High-Performance Battery-type Symmetric Supercapacitor". 1-18, 111 (2022).

[9] Attia, S. Y.; Mohamed, S. G.; Barakat, Y. F.; Hassan, H. H. and Zoubi, W.A.: Reviews in Inorganic Chemistry, "Supercapacitor electrode materials: addressing challenges in mechanism and charge storage". 53-88, 42 (2022).

[10] Bing, Y.; Zeng, Y.; Liu, C.; Qiao, L.; Sui, Y.; Zou, B.; Zheng, W. and Zou, G.: Sens. Actuators B Chem., "Assembly of hierarchical $ZnSnO_3$ hollow microspheres from ultra-thin nanorods and the enhanced ethanol-sensing performances". 370-377, 190 (2014).

[11] Wang, H.; Liu, X.-X.; Xie, J.; Duan, M. and Tang, J.-L.:Chin. Chem. Lett., "CO sensing properties of a cubic ZnSn (OH) 6 synthesized by hydrothermal method". 464-466, 27 (2016).

[12] Lo, M.-K.; Lee, S.-Y. and Chang, K.-S.: J. Phys. Chem. C, "Study of $ZnSnO_3$-nanowire piezophotocatalyst using two-step hydrothermal synthesis". 5218-5224, 119 (2015).

[13] Wang, Y.; Li, D.; Liu, Y. and Zhang, J.: Electrochim. Acta, "Self-assembled 3D $ZnSnO_3$ hollow cubes@ reduced graphene oxide aerogels as high capacity anode materials for lithium-ion batteries". 84-90, 203 (2016).
[14] Aksel, E. and Jones, J. L.: Sensors, "Advances in lead-free piezoelectric materials for sensors and actuators". 1935-1954, 10 (2010).
[15] Bauskar, D.; Kale, B. and Patil, P.:Sens. Actuators B Chem., "Synthesis and humidity sensing properties of $ZnSnO_3$ cubic crystallites". 396-400, 161 (2012).
[16] Zhang, Q.; Dandeneau, C. S.; Zhou, X. and Cao, G.: Adv. Mater., "ZnO nanostructures for dye-sensitized solar cells". 4087-4108, 21 (2009).
[17] Fan, H.; Zeng, Y.; Xu, X.; Lv, N. and Zhang, T.: Sens. Actuators B Chem., "Hydrothermal synthesis of hollow $ZnSnO_3$ microspheres and sensing properties toward butane". 170-175, 153 (2011).
[18] Huang, J.; Xu, X.; Gu, C.; Wang, W.; Geng, B.; Sun, Y. and Liu, J.: Sens. Actuators B Chem., "Size-controlled synthesis of porous $ZnSnO_3$ cubes and their gas-sensing and photocatalysis properties". 572-579, 171 (2012).
[19] Jin, C.; Kim, H.; An, S. and Lee, C.: Ceram. Int., "Highly sensitive H_2S gas sensors based on CuO-coated $ZnSnO_3$ nanorods synthesized by thermal evaporation". 5973-5978, 38 (2012).
[20] Zeng, Y.; Zhang, K.; Wang, X.; Sui, Y.; Zou, B.; Zheng, W. and Zou, G.: Sens. Actuators B Chem., "Rapid and selective H_2S detection of hierarchical $ZnSnO_3$ nanocages". 245-250, 159 (2011).
[21] Zeng, Y.; Zhang, T.; Fan, H.; Lu, G. and Kang, M.: Sens. Actuators B Chem., "Synthesis and gas-sensing properties of $ZnSnO_3$ cubic nanocages and nanoskeletons". 449-453, 143 (2009).
[22] Wu, J. M.; Chen, C.-Y.; Zhang, Y.; Chen, K.-H.; Yang, Y.; Hu, Y.; He, J.-H. and Wang, Z. L.: Acs Nano, "Ultrahigh sensitive piezotronic strain sensors based on a $ZnSnO_3$ nanowire/microwire". 4369-4374, 6 (2012).
[23] Gou, H.; Gao, F. and Zhang, J.: Comput. Mater. Sci., "Structural identification, electronic and optical properties of $ZnSnO_3$: First principle calculations". 552-555, 49 (2010).
[24] Xing, G.; Lu, Y.; Tian, Y.; Yi, J.; Lim, C.; Li, Y.; Li, G.; Wang, D.; Yao, B. and Ding, J.: AIP Adv., "Defect-induced magnetism in undoped wide band gap oxides: Zinc vacancies in ZnO as an example". 022152, 1 (2011).
[25] Wu, X.; Liu, X.; Wei, J.; Ma, J.; Deng, F. and Wei, S.: Int. J. Nanomedicine, "Nano-TiO_2/PEEK bioactive composite as a bone substitute material: in vitro and in vivo studies". 1215, 7 (2012).
[26] Inagaki, M.; Kuroishi, T.; Yamashita, Y.; Urata, M. and Anorg, Z.: Allg. Chem., "Syntheses of $MSn(OH)_6$ by coprecipitation and of $MSnO_3$ by thermal decomposition (M = Mg, Co, Zn, Mn, Cd, Ca, Sr, Ba)". 193-202, 527 (1985).
[27] Cun, W.; Xinming, W.; Jincai, Z.; Bixian, M.; Guoying, S.; Ping'an, P. and Jiamo, F.: J. Mater. Sci., "Synthesis, characterization and photocatalytic property of nano-sized Zn_2SnO_4". 2989-2996, 37 (2002).
[28] Wohlfahrt-Mehrens, M.; Schenk, J.; Wilde, P.; Abdelmula, E.; Axmann, P. and Garche, J.: J. Power Sources, "New materials for supercapacitors". 182-188, 105 (2002).
[29] Lokhande, C.; Gujar, T.; Shinde, V.; Mane, R. S. and Han, S.-H.: Electrochem. Commun., "Electrochemical supercapacitor application of pervoskite thin films". 1805-1809, 9 (2007).

[30] Ge, N.-N.; Liu, C.-M.; Cheng, Y.; Chen, X.-R. and Ji, G.-F.: Physica B: Condensed Matter, "First-principles calculations for elastic and electronic properties of $ZnSnO_3$ under pressure". 742-748, 406 (2011).
[31] Zeng, Y.; Zhang, T.; Wang, L.; Wang, R.; Fu, W. and Yang, H.: J. Phys. Chem. C, "Synthesis and ethanol sensing properties of self-assembled monocrystalline ZnO nanorod bundles by poly (ethylene glycol)-assisted hydrothermal process". 3442-3448, 113 (2009).
[32] Miyauchi, M.; Liu, Z.; Zhao, Z.-G.; Anandan, S. and Hara, K.: Chem. Commun., "Single crystalline zinc stannate nanoparticles for efficient photo-electrochemical devices". 1529-1531, 46 (2010).
[33] Baruah, S. and Dutta, J.: Sci. Technol. Adv, Mater., "Zinc stannate nanostructures: hydrothermal synthesis". 013004, 12 (2011).
[34] Inaguma, Y.; Sakurai, D.; Aimi, A.; Yoshida, M.; Katsumata, T.; Mori, D.; Yeon, J. and Halasyamani, P. S.: J. Solid State Chem., "Dielectric properties of a polar $ZnSnO_3$ with $LiNbO_3$-type structure". 115-119, 195 (2012).
[35] Men, H.; Gao, P.; Zhou, B.; Chen, Y.; Zhu, C.; Xiao, G.; Wang, L. and Zhang, M.: Chem. Commun., "Fast synthesis of ultra-thin $ZnSnO_3$ nanorods with high ethanol sensing properties". 7581-7583, 46 (2010).
[36] Chen, Y.; Qu, B.; Mei, L.; Lei, D.; Chen, L.; Li, Q. and Wang, T.: J. Mater. Chem., "Synthesis of $ZnSnO_3$ mesocrystals from regular cube-like to sheet-like structures and their comparative electrochemical properties in Li-ion batteries". 25373-25379, 22 (2012).
[37] Sim, C.-K.; Majid, S. R. and Mahmood, N. Z.: Microchem. J., "$ZnSnO_3$/mesoporous biocarbon composite towards sustainable electrode material for energy storage device". 105968, 164 (2021).
[38] C.-K. Sim, ; Majid, S. R. and Mahmood, N. Z.: J. Energy Storage, "Synthesis of highly porous carbon/$ZnSnO_3$ composite and its electrochemical properties". 101843, 32 (2020).
[39] Morad, M. M.; Attia, S. Y.; Mohamed, S. G.; Moharam, M. M.; AbouShahba, R. M. and Rashad, M. M.: Al-Azhar Bulletin of Science, "PREPARATION AND ELECTROCHEMICAL BEHAVIOR OF THE ACTIVATED CARBON FROM POMEGRANATE PEELS AS ENERGY-STORAGE MATERIALS". 1-9, 31 (2020).
[40] Li, X.; Shen, J.; Li, N. and Ye, M.: J. Power Sources, "Fabrication of γ-MnS/rGO composite by facile one-pot solvothermal approach for supercapacitor applications". 194-201, 282 (2015).
[41] Mohamed, S. G.; Hussain, I. and Shim, J.-J.: Nanoscale, "One-step synthesis of hollow C-$NiCo_2S_4$ nanostructures for high-performance supercapacitor electrodes". 6620-6628, 10 (2018).
[42] Chen, T.; Tang, Y.; Qiao, Y.; Liu, Z.; Guo, W.; Song, J.; Mu, S.; Yu, S.; Zhao, Y. and Gao, F.: Sci. Rep., "All-solid-state high performance asymmetric supercapacitors based on novel MnS nanocrystal and activated carbon materials". 23289, 6 (2016).
[43] Dai, C.-S.; Chien, P.-Y.; Lin, J.-Y.; Chou, S.-W.; Wu, W.-K.; Li, P.-H.; Wu, K.-Y. and Lin, T.-W.: ACS Appl. Mater. Interfaces, "Hierarchically structured Ni_3S_2/carbon nanotube composites as high performance cathode materials for asymmetric supercapacitors". 12168-12174, 5 (2013).

[44] D. Kong, ; C. Cheng, ; Y. Wang, ; J. I. Wong, ; Y. Yang, and H. Y. Yang, : J. Mater. Chem. A, "Three-dimensional Co_3O_4@C@Ni_3S_2 sandwich-structured nanoneedle arrays: towards high-performance flexible all-solid-state asymmetric supercapacitors". 16150-16161, 3 (2015).

[45] Abdel-Aal, S. K.; Attia, S. Y. and Mohamed, S. G.: J. Electron. Mater., "Facile Synthesis of Mn_3O_4-rGO Nanocomposite As an Efficient Electrode Material for Application in Supercapacitors". 4977-4986, 48 (2019).

[46] Qin, Y.-l.; Zhang, F.-f.; Du, X.-c.; Huang, G.; Liu, Y.-c. and Wang, L.-m.: J. Mater. Chem. A, "Controllable synthesis of cube-like $ZnSnO_3$@TiO_2 nanostructures as lithium ion battery anodes". 2985-2990, 3 (2015).

[47] Zhang, S.; Fan, Q.; Gao, H.; Huang, Y.; Liu, X.; Li, J.; Xu, X. and Wang, X.: J. Mater. Chem. A, "Formation of Fe_3O_4@MnO_2 ball-in-ball hollow spheres as a high performance catalyst with enhanced catalytic performances". 1414-1422, 4 (2016).

[48] Ito, Y.; Cong, W.; Fujita, T.; Tang, Z. and Chen, M.: Angew. Chem. Int. Ed., "High catalytic activity of nitrogen and sulfur co-doped nanoporous graphene in the hydrogen evolution reaction". 2131-2136, 54 (2015).